Near-field Simulation of Ground Motions of 16 April 2013 Iran-Pakistan Border Earthquake Using Semi-Empirical Approach

Chenna Rajaram[1] and Ramancharla Pradeep Kumar[2]*

1. Ph.D. Scholar, Civil Engineering, Earthquake Engineering Research Centre, International Institute of Information Technology, Hyderabad, India
2. Professor of Civil Engineering, Earthquake Engineering Research Centre, International Institute of Information Technology, Hyderabad, India,
* Corresponding Author; email: ramancharla@iiit.ac.in

Received: 19/10/2014
Accepted: 20/10/2015

ABSTRACT

The 7.8 M earthquake occurred in south east Iran on 16 April 2013 at 10:44:20 UTC. This earthquake was the most massive earthquake in last 50 years, with tremors felt across Pakistan, Oman and UAE. According to BHRC (Iranian Building and Housing Research Center) report, this event was recorded by 33 digital accelerographs in Iran Strong Ground Motion Network. The peak acceleration was recorded in Sabz Gazz seismic station. This study presents simulation of near-field ground motions of the 2013 Iran earthquake. For this purpose, five seismic stations are selected to simulate ground motions using semi-empirical approach. Hamzehloo and Mahood (2012) attenuation relationship for south east Iran is used to obtain acceleration waveform envelope function. A comparison is done on characteristics of observed and simulated ground motions. The simulated results are satisfactory at many of the seismic stations. It is concluded that higher frequencies (2-10 Hz) of simulated ground motions match with observed ground motions.

Keywords:
Simulated ground motion;
Envelope function;
Attenuation relationship;
Semi-empirical approach

1. Introduction

The M 7.8 earthquake occurred in south east Iran on 16 April 2013 at 10:44:20 UTC. The hypocenter of the earthquake is located at 28.107° N, 62.053° E which is about 83 km towards north of Khash, Iran at an intermediate depth of 82 km [1]. This event was occurred by the collisions of the Arabian and Indian tectonic plates with Eurasian plate. The number of casualties was one in Iran and 35 in Pakistan. Around 1000 mud-and-sun-dried brick houses were collapsed during the earthquake. According to Iranian Building and Housing Research Center (BHRC) report, the event recorded at 33 seismic stations. The peak acceleration was recorded 0.196 g at Sabz-Gazz seismic station. Present study simulates near-field ground motions of the 2013 Iran earthquake. A comparison has made on characteristics of ground motions between observed and simulated ground motions at five near-field seismic stations.

2. An Overview of Seismo-Tectonic of South-East Iran

The Makran subduction zone is located on offshore of Iran and Pakistan in Arabian Sea. This zone on the Arabian plate is converging towards the north-northeast at a rate of 37 mm/yr with respect to the Eurasian plate [1]. The Arabian plate is subducting beneath the Eurasian plate at the Makran coast of Pakistan and Iran [2]. This subducted Arabian plate is seismically active at deeper

depths of about 160 km [2]. Northward motion of the Arabian plate consists of: a) folding and reverse faulting, b) strike-slip faulting, and c) subduction beneath the Makran region [3]. However, distribution of relative velocities between the Arabian plate and the Eurasian plate is non-uniform in Iran. GPS studies show that the Arabian plate moves at 2.1-2.5 cm/yr towards north, 1.9 cm/yr towards east, and 0.8 cm/yr towards west [3]. The frequency of moderate to large earthquake events within the subducted Arabian plate is less compared with other subduction regions worldwide. The mechanism of the event is similar to earthquakes that occurred on 18 April 1983 (Mw 6.7) and 18 January 2011 (Mw 7.2) [4].

Earthquake focal mechanisms suggest that the convergence between the Arabia and the Eurasia plates has been accommodated mainly right-lateral strike-slip faults in the north west of Iran. On the other hand, right-lateral faulting in Iran region is not continuous but consists of several discontinuous fault segments. Three of these segments ruptured during earthquakes in 1930, 1966 and 1976 [3]. In eastern and central Iran, the number of active faults is more and the fault systems are different from other parts of Iran due to their orientation and geometric characteristics. The eastern limit of the Makran is marked by the Chaman and Ornach-Nal faults of Pakistan. The NNW trending Zendan-Minab-Palami fault zone marks the western limit of the Makran subduction zone and connects the western Makran to the eastern Zagros deformation domain [3]. The epicenter and focal mechanism solution of the earthquake are shown in Figure (1). The seismicity data of Iran is obtained from National Earthquake Information Centre, USA since 1898, Figure (2) [7].

3. Literature Review

The Bam earthquake is one of the most destructive earthquakes in south eastern part of Iran. The accelerogram recorded at Bam station is large and relatively long period pulses. The recorded ground motions were simulated using Stochastic Finite Fault Simulation technique [5]. The observed and simulated spectra show a good agreement within the intermediate and high frequencies. Based on the relative arrival time of rupture front, P and S waves, rupture velocity was estimated as 2.5 km/s [6]. The same technique is used to generate ground

Figure 1. Event location of 16 April 2013 Iran earthquake and focal mechanism solution of the earthquake (Star: epicenter of the earthquake). The data source is taken from USGS.

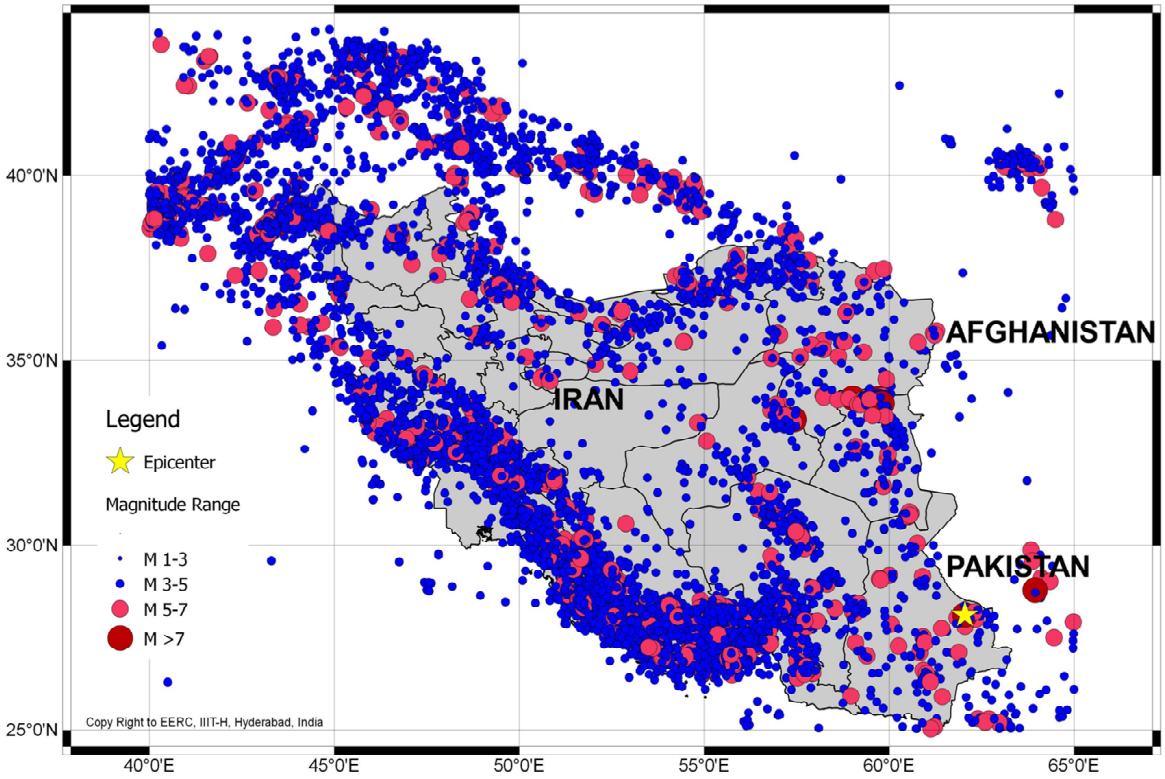

Figure 2. Seismicity data of Iran obtained from NEIC, USA since 1898 [7].

motions for 2010 Rigan earthquake, south-east Iran. The value of *Qs* estimated in the range of 1-24 Hz and the value of kappa is estimated as 0.06 for Rigan region. A quiet satisfactory agreement was found between observed and simulated ground motion parameters such as PGA, PGV, and PGD frequencies [8]. The frequency dependent parameter *Qs* for Rigan region is similar to north-eastern Mexico [9-11]. Though the past earthquakes occurred in the range of 300 km from epicenter of the 2013 Iran earthquake, the same seismological parameters cannot be used to generate ground motions. For this purpose, semi-empirical approach is used to obtain ground motions at five near-field seismic stations. The methodology of semi-empirical approach is describing in the subsequent section.

4. Methodology

The synthetic accelerograms are generated using semi-empirical simulation technique by Midorikawa, which is based on stochastic simulation by Boore and Empirical Green's function by Irikura [12-17]. The reason for the selection of this semi-empirical technique is that it does not require many seismological parameters and it is fast to compute. This method has some advantages, e.g. it does not require; i) the actual ground motion record of small events, ii) the stress-drop parameter as in the case of empirical Green's function technique [13], iii) the *Q* structure; and iv) the fault plane solution as in the case of the composite source model [18]. The semi-empirical simulation method is as follows:

In the stochastic simulation technique, the white Gaussian noise of zero expected mean and variance chosen such that it gives unit spectral amplitude and the same has been passed through the number of filters representing the earthquake processes [12]. The shape of acceleration spectrum $A(f)$ at a site located at a hypo-central distance R is given as:

$$A(f) = S(f)\,P(f)\left[e^{(-\pi fR/\beta Q)} / R\right] \quad (1)$$

where $S(f)$ represents the source acceleration spectrum [19], $P(f)$ represents attenuation of high frequencies at near site [12], R is hypo-central distance from source to site in km, β is shear wave velocity in km/sec and Q frequency dependent quality factor.

$$S(f) = (2\pi f)^2 / \left[1 + (f / f_c)^2\right] \quad (2)$$

$$P(f)=1/\left[1+(f/f_m)\right] \quad (3)$$

where f_c is the corner frequency, and f_m represents high-frequency cutoff range of the high-cut filter. The geophysical parameters for the above-mentioned earthquake are shown in Table (1).

Table 1. Geophysical parameters of the 16 April 2013, Iran earthquake.

Parameters	Values
Magnitude	7.8
Type of Fault	Thrust Fault
Name of Fault	Saravan Fault
Strike Angle	231.5°
Dip Angle	61.1°
Shear Wave Velocity, β (km/s)	3.5
Rupture Velocity, V_r (km/sec)	3.3
Seismic Moment, M_o (N.m)	4.85×10^{21} (Source: USGS)
Frequency dependent Quality factor	$Q(f)=52.6f^{1.2}$
Stress Drop, Δσ (MPa)	4
Maximum Frequency (f_{max})	$7.31 \times 10^3 M_o^{(-0.12)}$
Time Interval (s)	0.005
Attenuation: $\log_{10}(a) = 2.615 + 0.31(Mw-6) - 0.0455(Mw-6)^2 - 0.0126(r^2+h^2) + 0.33$	
Corner frequency (f_o)	$4.9 \times 10^6 \beta(\Delta\sigma/M_o)^{0.33}$

It is observed that stochastic simulation technique requires proper windowing of the obtained record, which is based on kinematic representation of model of rupture. Such window can be obtained by the semi-empirical technique in the form of resultant envelope of accelerogram. The finite fault is divided into several sub-faults, and the energy is released in the form of acceleration envelope whenever rupture approaches the center of the elements. The acceleration envelope waveform $e_{ij}(t)$ is determined by Kameda and Sugito [20] and further modified by Joshi [17]. The final acceleration record $ac_{ij}(t)$, is the product of acceleration record from stochastic simulation technique with envelope function from semi-empirical technique, Eq. (5).

$$e_{ij}(t)=T_{ss}\left[a_{ij}\frac{t}{T_d}e^{\left(1-\frac{t}{T_d}\right)}\right] \quad (4)$$

$$ac_{ij}(t)=e_{ij}(t)\times A_{ij}(t) \quad (5)$$

where, a_{ij} is empirical relation of peak ground acceleration, T_{ss} is transmission coefficient of incident shear wave. It contributes significantly to the shaping of attenuation rate of the PGA with respect to the distance from the source. For the shallow focus earthquakes, the transmission coefficient is approximately equal to 1.0. T_d is the duration parameter [17]. The present paper considers the ground motion attenuation relationship for eastern Iran [21]. Eq. (6) shows the attenuation relationship for eastern Iran region. The envelope function-attenuation relationship and duration parameter used in this analysis are given in Eqs. (6) and (7).

$$\log_{10}(a)=2.615+0.31(M_w-6)- 0.0455(M_w-6)^2-0.0126(r_{jb}^2+h^2)+0.33 \quad (6)$$

$$T_d=0.0015\times 10^{0.5M_L}+1.08R^{0.41} \quad (7)$$

A vector notation has been used to resolve acceleration record into E-W and N-S horizontal components. The direction of acceleration component from each sub-fault is defined by line joining center of sub-fault to the recording station. Figure (3) illustrates simulation of E-W and N-S components of earthquake ground motion. The above method has been used to generate synthetic ground motions of the 16 April 2013 Iran earthquake. The flowchart of semi-empirical approach is shown in Figure (4). A MATLAB code is written to obtain synthetic ground motion at five seismic stations. The location of seismic stations is shown in Figure (5). The description on characteristics of observed and analytical ground motion records at above seismic stations are as follows:

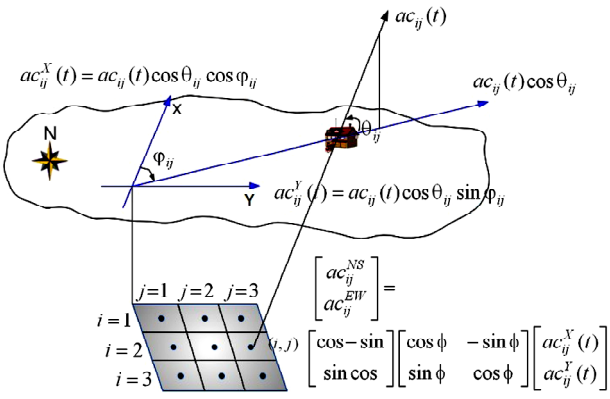

Figure 3. Simulation of E-W and N-S components of earthquake ground motion (Data Source: [17]).

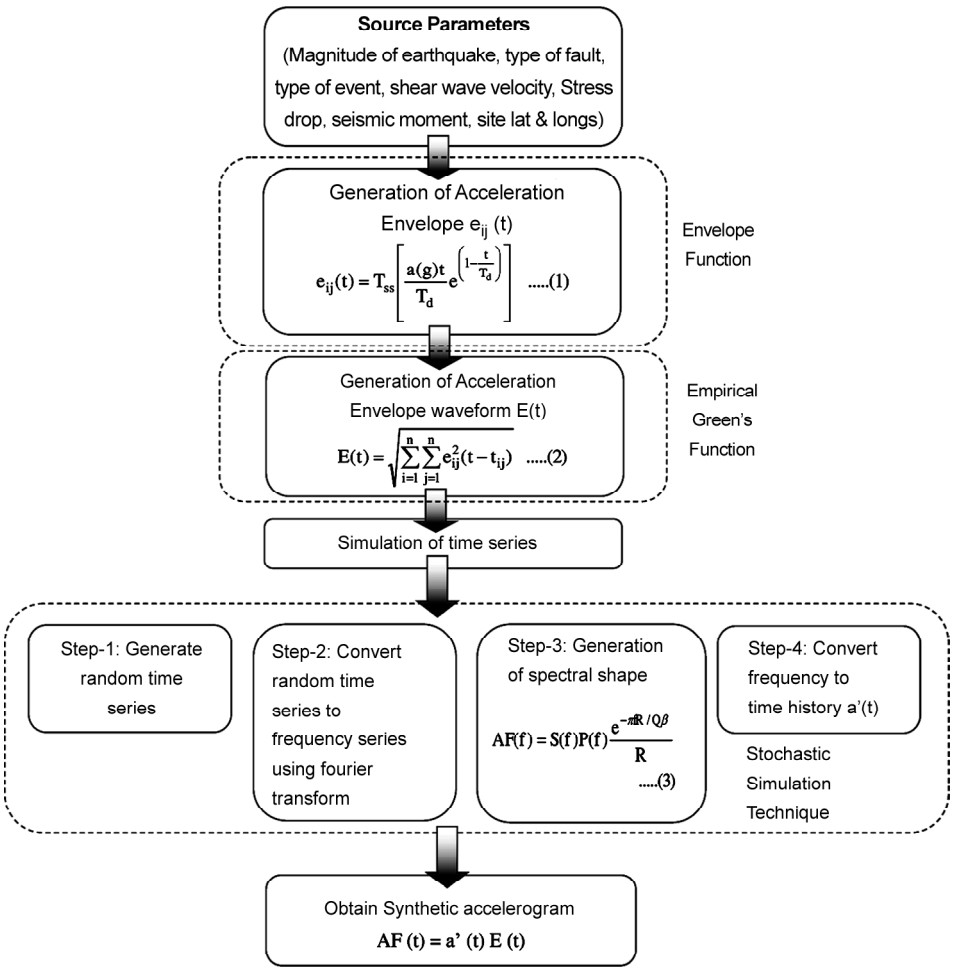

Figure 4. Flow chart for generating synthetic ground acceleration using semi-empirical approach.

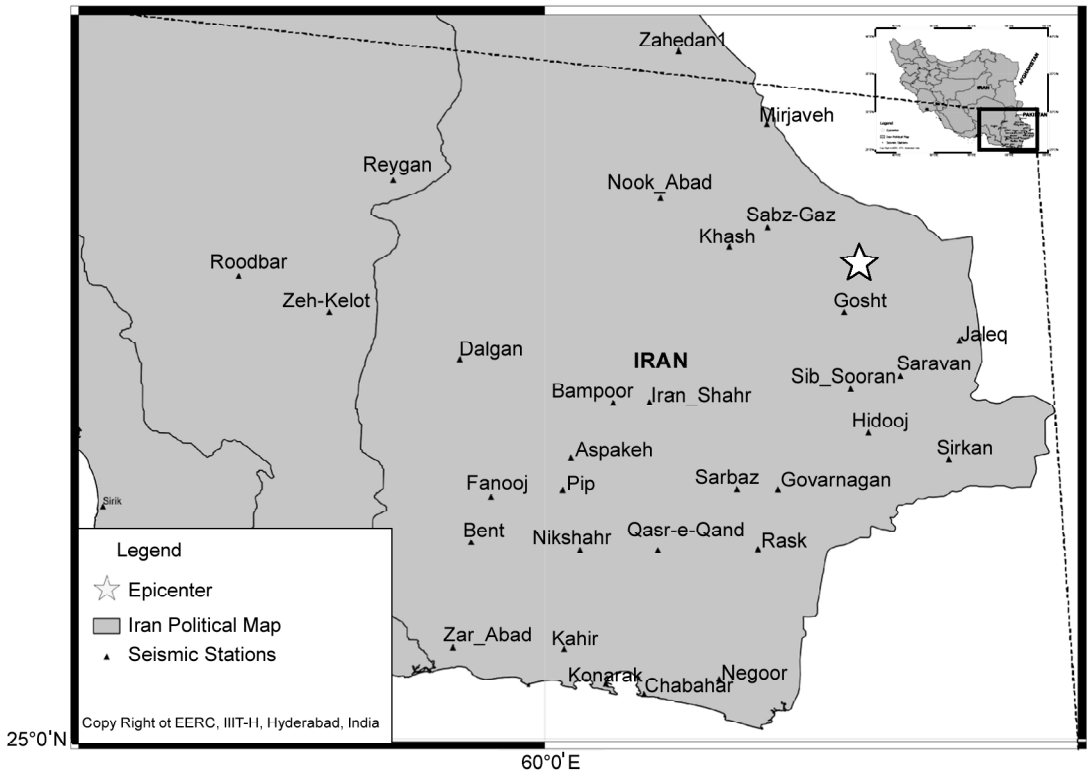

Figure 5. The location of seismic stations of the 16 April 2013 Iran earthquake (Source Data: BHRC).

5. Results and Discussion

5.1. Observed Ground Motion Records:

The event was digitally recorded at 33 seismic stations by BHRC. All strong motion records have 200 Hz sampling rate (dt = 0.005 s). Seismic stations (Gosht, Saravan, Sib Sooran, Hidooj and Mirjaveh) located around 150 km are considered as near-field seismic stations. Figure (6) shows observed and simulated ground motion records of the earthquake. Figure (7) shows Fourier amplitude spectra of corresponding ground motion. The description of characteristics of near-field ground motion at above seismic stations is as follows:

Gosht: The Gosht station (61.956 E, 27.79 N) is located 53 km from epicenter of the earthquake. Peak ground accelerations were 0.152 g, 0.164 g along fault parallel (FP) and fault normal (FN) directions respectively. The high-acceleration portion of the record lasts 1.8 s and 2.0 s on FP and

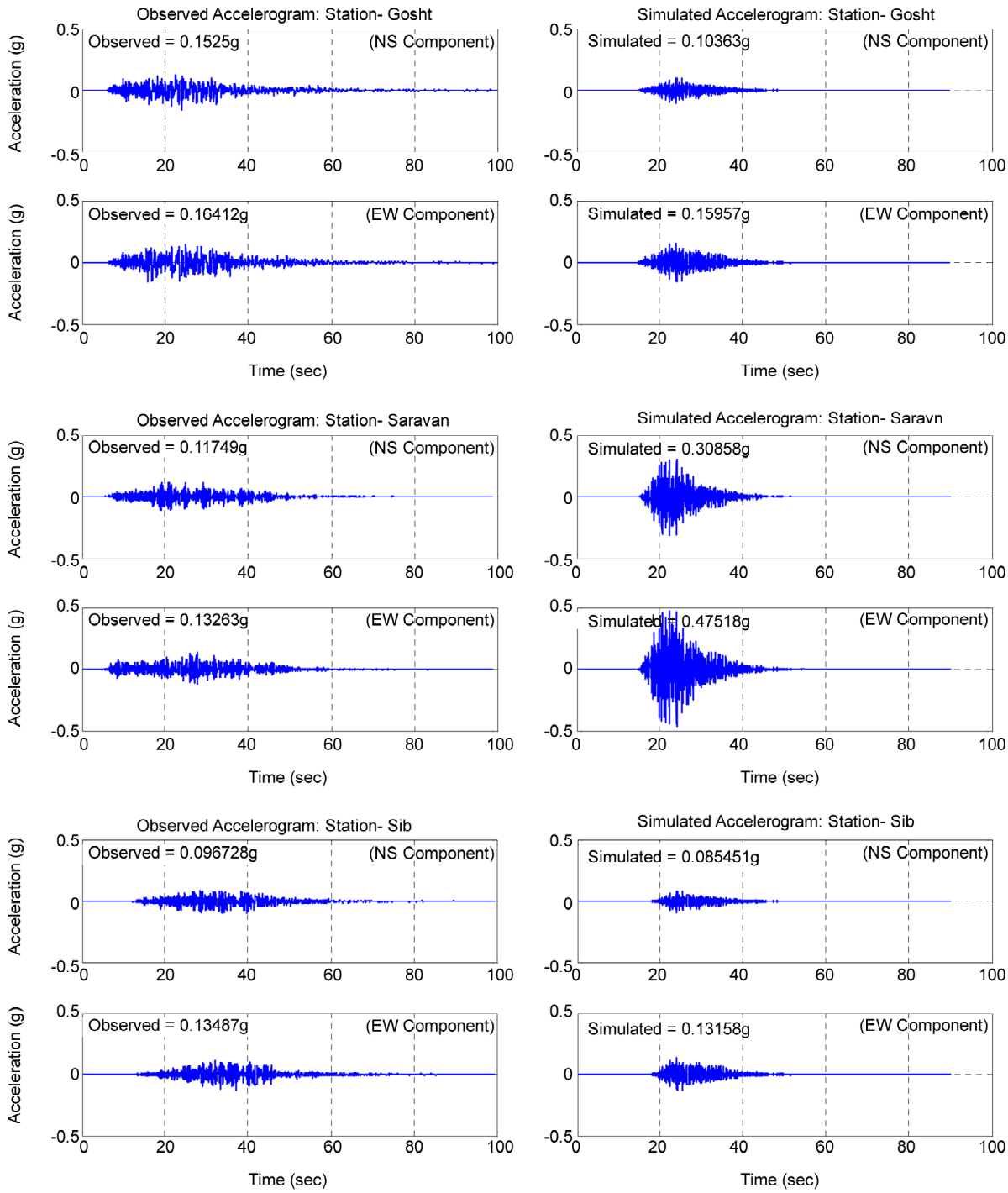

Figure 6. Observed and simulated ground motions at Gosht, Saravan, Sib Sooran, Hidooj and Mirjaveh seismic stations.

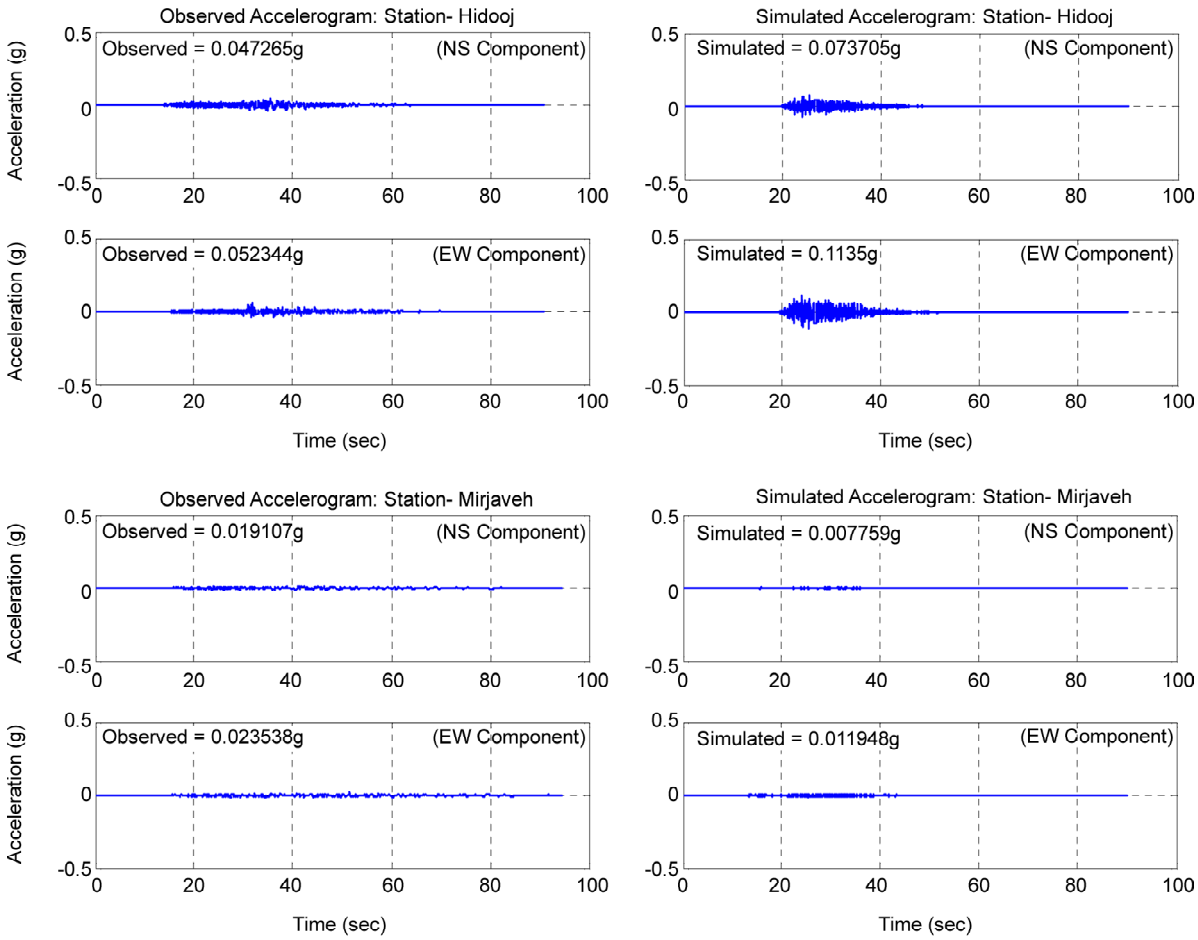

Figure 6. Continue.

FN components respectively. High-amplitude portion of the record lasts longer on FN component than on FP component. The PGA, PGV and PGD values of FN and FP components are shown in Table (2). The decay of Fourier amplitude is similar in both FP and FN components. Trifunac and Brady duration is used to calculate duration of ground motions [22]. The duration values are 144.12 s and 132.2 s on FP and FN components respectively.

Saravan: The Saravan station (62.324 E, 27.373 N) is located 98 km from epicenter of the earthquake. Peak ground accelerations were 0.117 g, 0.133 g along FP and FN directions respectively. The high-acceleration portion of the record lasts 1.2 s and 1.65 s on FP and FN components respectively. High-amplitude portion of the record lasts longer on the FN component than on the FP component. The decay of Fourier amplitude is similar in both FP and FN components. The duration values are 123.9 s and 143.1 s on FP and FN components respectively.

Sib Sooran: The Sib Sooran station (61.998 E, 27.286 N) is located 107 km from epicenter of the earthquake. Peak ground accelerations were 0.097 g, 0.135 g along FP and FN directions respectively. The high-acceleration portion of the record lasts 2.1 s and 1.5 s on FP and FN components respectively. High-amplitude portion of the record lasts longer on the FP component than on the FN component. The decay of Fourier amplitude is similar in both FP and FN components. The duration values are 111.7 s and 93.84 s on FP and FN components respectively.

Hidooj: The Hidooj station (62.114 E, 27.0 N) is located 138 km from epicenter of the earthquake. Peak ground accelerations were 0.047 g, 0.052 g along FP and FN directions respectively. The high-acceleration portion of the record lasts 3.4 s and 2.8 s on FP and FN components respectively. High-amplitude portion of the record lasts longer on the FP component than on the FN component. The decay of Fourier amplitude is similar in both FP and FN components. The duration values are 129.78 s and 126.78 s on FP and FN components respectively.

Mirjaveh: The Mirjaveh station (61.451 E, 29.019 N) is located 110 km from epicenter of the

earthquake. Peak ground accelerations were 0.019 g, 0.024 g along FP and FN directions respectively. The high-acceleration portion of the record lasts 2.3 s and 1.7 s on FP and FN components respectively. High amplitude portion of the record lasts longer on the FP component than on the FN component. The decay of Fourier amplitude is similar in both FP and FN components. The duration values are 220.76 s and 234.84 s on FP and FN components respectively.

5.2. Simulated Ground Motion Records

Gosht: The PGAs of observed and simulated ground motion are 0.152 g, 0.164 g and 0.103 g, 0.159 g along FP and FN directions respectively. These values underestimate the observed values. A good match is observed in the Fourier amplitude spectrum

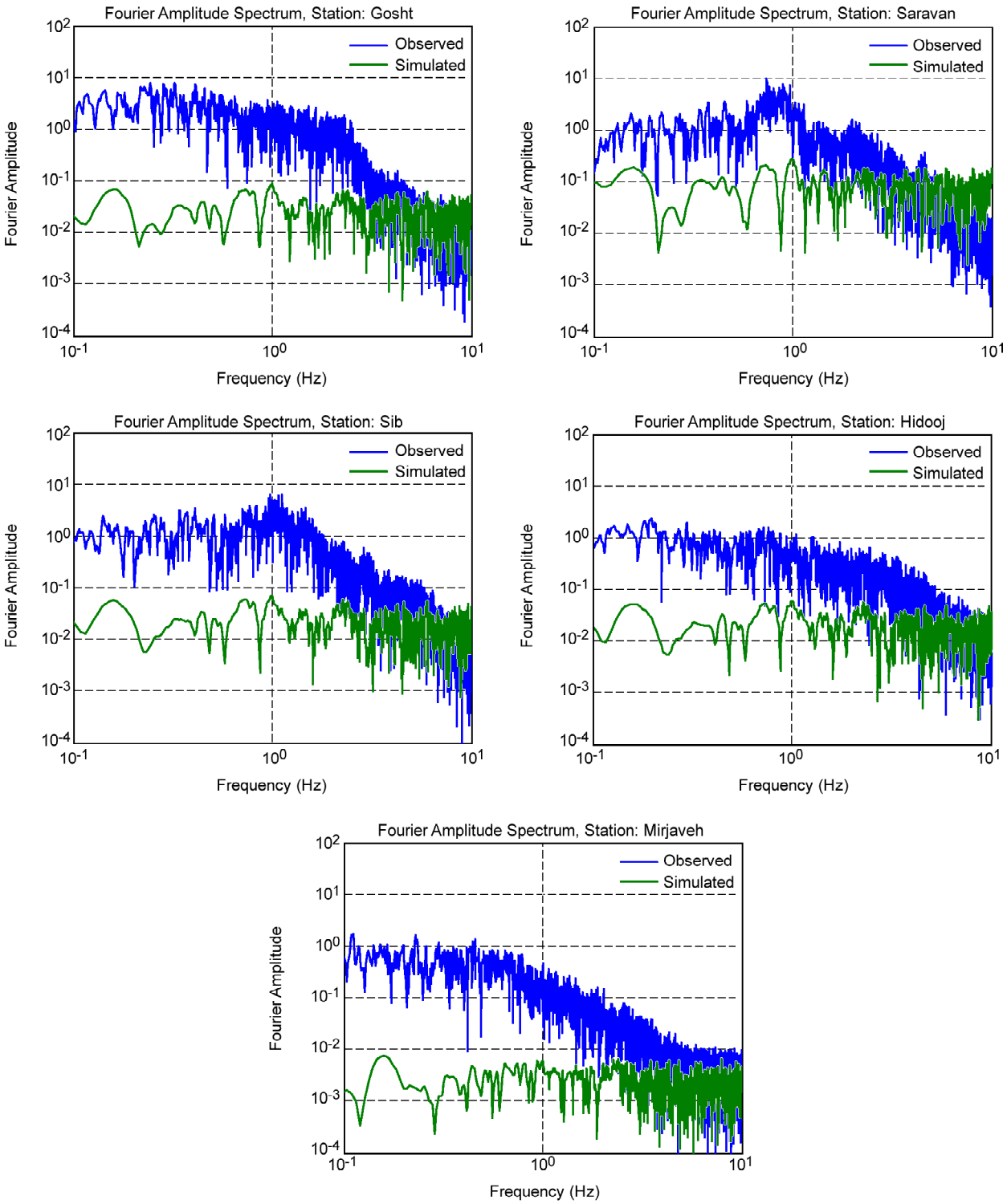

Figure 7. Observed and simulated Fourier amplitude spectra at Gosht, Saravan, Sib Sooran, Hidooj and Mirjaveh seismic stations.

Table 2. Comparison among PGA, PGV, PGD and duration of observed and simulated ground motions of the 16 April 2013, Iran earthquake.

Station	Epicentral Distance (km)	PGA (g)		PGV (m/s)		PGD (m)		Duration (s)	
		FP	FN	FP	FN	FP	FN	FP	FN
		Observed Ground Motions							
Gosht	53	0.152	0.164	1.02	0.95	23	11.24	48.04	44.07
Saravan	98	0.117	0.133	0.36	0.66	4.47	9.34	41.30	47.70
Sib Sooran	107	0.097	0.135	0.407	0.44	8.80	11.33	37.23	31.28
Hidooj	138	0.047	0.052	0.305	0.302	8.77	6.14	43.26	42.26
Mirjaveh	110	0.019	0.024	0.215	0.172	1.33	11.16	73.59	78.28
		Simulated Ground Motions							
Gosht	53	0.103	0.16	0.044	0.082	1.67	5.34	15	18
Saravan	98	0.30	0.47	0.15	0.28	6.23	7.86	13.28	21.54
Sib Sooran	107	0.085	0.131	0.028	0.087	0.80	1.56	14.72	16.86
Hidooj	138	0.073	0.11	0.02	0.073	0.58	0.92	14.66	18.97
Mirjaveh	110	0.007	0.011	0.0045	0.09	0.255	0.72	27.16	32.56

ranges 3-10. The duration values are calculated using Trifunac and Brady relation and those are 15.0 s and 18.0 on FP and FN components.

Saravan: The PGAs of observed and simulated ground motion are 0.117 g, 0.133 g and 0.3 g, 0.47 g along FP and FN directions respectively. These values overestimate the observed values. A good match is observed in the Fourier amplitude spectrum ranges 1-6 Hz. The duration values are calculated using Trifunac and Brady relation and those are 13.28 s and 21.54 on FP and FN components.

Sib Sooran: The PGAs of observed and simulated ground motion are 0.097 g, 0.135 g and 0.085 g, 0.131 g along FP and FN directions respectively. These values underestimate the observed values. A good match is observed in the Fourier amplitude spectrum ranges 3-10 Hz. The duration values are calculated using Trifunac and Brady relation and those are 14.72 s and 16.86 on FP and FN components.

Hidooj: The PGAs of observed and simulated ground motion are 0.047 g, 0.052 g and 0.073 g, 0.11 g along FP and FN directions respectively. These values underestimate the observed values. A good match is observed in the Fourier amplitude spectrum ranges 2-10 Hz. The duration values are calculated using Trifunac and Brady relation and those are 14.66 s and 18.97 on FP and FN components.

Mirjaveh: The PGAs of observed and simulated ground motion are 0.019 g, 0.024 g and 0.007 g, 0.011 g along FP and FN directions respectively. These values underestimate the observed values. A good match is observed in the Fourier amplitude spectrum ranges 2-10 Hz. The duration values are calculated using Trifunac and Brady relation and those are 27.16 s and 32.56 on FP and FN components.

A comparative study of observed and simulated ground motions of the 2013 Iran earthquake reveals that the method has effectively modeled at selected seismic stations. Maximum PGA from simulated data is observed at Saravan seismic station, whereas actual data indicates that maximum PGA at Gosht seismic station. This may be due to proximity of Ghost seismic station to the seismic fault. It is assumed that the rupture front propagates from South East to North West of Saravan fault in the simulation of ground motion. The difference between observed and simulated results may be due to not only insufficiency of ground motion prediction equation (GMPE) but also simulation method, since the analysis does not account the site effect resulted from the response of the multi-layered ground near the surface to the incoming seismic waves. This difference can be minimized based on goodness-of-fit criteria proposed by Kristekova et al. [23], which will become future scope of the study. The simulated results are satisfactory at many of the seismic stations. It is concluded that higher frequencies (2-10 Hz) of simulated ground motions match with observed ground motions.

6. Conclusions

This paper presents simulation of ground motions of 16 April 2013 Iran earthquake. For the purpose of simulation, a MATLAB code is written to obtain

synthetic ground motions. In this study, five near-field seismic stations are selected. Hamzehloo, H., and Mahood, M. attenuation relationship for south east Iran is used to obtain acceleration waveform envelope function. A comparison is done on characteristics of observed and simulated ground motions. Maximum PGA from simulated data is observed at Saravan seismic station, whereas actual data indicates that maximum PGA is at Gosht seismic station. This may be due to proximity of Ghost seismic station to the seismic fault. The simulated results are satisfactory at many of the seismic stations. It is concluded that higher frequencies (2-10 Hz) of simulated ground motions match with observed ground motions.

References

1. Data source: USGS, http://comcat.cr.usgs.gov/earthquakes/eventpage/usb000g7x7#summary, dated 8 February 2015.

2. United States of Geological Survey, http://www.usgs.gov/, dated 2 July 2014.

3. Hessami, K. and Jamali, F. (2006) Explanatory notes to the map of major active faults of Iran. *Journal of Seismology and Earthquake Engineering*, **8**(1), 1-11.

4. Bhaskar, K., Nankali, H., Malik, P., Yadav, R.K., and Gahalaut, V.K. (2014) Coseismic offsets due to intermediate depth 16 April 2013 southeast Iran earthquake. *Bull. Seism. Soc. Am.*, **104**(3), 1562-1566.

5. Shojataheri, J. and Ghofrani, H. (2007) Stochastic finite-fault modeling of strong ground motions from the 26 December 2003 bam, Iran, earthquake. *Bull. Seism. Soc. Am.*, **97**, 1950-1959.

6. Shojataheri, J., Naserieh, S., and Ghafoorian, H. (2005) The 2003 Bam, Iran, earthquake: an interpretation of the strong motion records. *Earthquake Spectra*, **21**(S1), S181- S206.

7. Data Source: NEIC

8. Safarshahi, M., Rezapour, M., and Hamzehloo, H. (2013) Stochastic finite-fault modeling of ground motion for the 2010 Rigan earthquake, southeastern Iran, *Bull. Seism. Soc. Am.*, **103**(6), 223-235.

9. Castro, R.R., Condori, C., Romero, O., Jacques, C., and Suter, M. (2008) Seismic attenuation in northeastern Sonora, Mexico. *Bull. Seism. Soc. Am.*, **98**, 722-732.

10. Polatidis, A., Kiratzi, A., Hatzidimitriou, P., and Margaris, B. (2003) Attenuation of shear waves in the back-arc region of the Hellenic arc for frequencies from 0.6 to 16 Hz. *Tectonophysics*, 367, 29-40.

11. Castro, R.R., Monachesi, G., Mucciareli, M., Trojani, L., and Pacor, F. (1999) P and S wave attenuation in the region of Marche, Italy. *Tectonophysics*, **302**, 123-132.

12. Boore, D.M. (1983) Stochastic simulation of high frequency ground motion based on seismological models of radiated spectra. *Bull. Seism. Soc. Am.*, **73**, 1865-1894.

13. Irikura, K. (1986) Prediction of strong acceleration motion using empirical Green's function. *Proc. 7th Japan Earthquake Engineering Symposium*, 151-156.

14. Midorikawa, S. (1993) Semi-empirical estimation of peak ground acceleration from large earthquakes. *Tectonophysics*., **218**, 287-295.

15. Joshi, A., Singh, S., and Kavita, G. (2001) The simulation of ground motions using envelope summations. *Pure Appl. Geophys.*, **158**, 877-901.

16. Joshi, A. and Midorikawa, S. (2004) A simplified method for simulation of strong ground motion using finite rupture model of the earthquake source. *Journal of Seismology*, **8**, 467-484.

17. Joshi, A., Pushpa K., Sandeep, S., and Sharma, M.L. (2012) Near-field and far-field simulation of accelerograms of Sikkim earthquake of September 18, 2011 using modified semi-empirical approach. *Natural Hazards*, **64**, 1029-1054.

18. Zeng, Y., Anderson, J.G., and Yu, G. (1994a) A composite source model for computing realistic synthetic strong ground motions. *Geophysical Research Letters*, **21**, 725-728.

19. Brune, J.N. (1970) Tectonic stress and spectra

of seismic shear waves from earthquakes. *J. Geophys. Res.*, **75**, 4997-5009.

20. Kameda, H. and Sugito, M. (1978) Prediction of strong earthquake motions by evolutionary process model. *Proc. 6th Japan Earthquake Engineering Symposium*, 41-48.

21. Hamzehloo, H. and Mahood, M. (2012) Ground-motion attenuation relationship for east central Iran. *Bull. Seism. Soc. Am.*, **102**(6), 2677-2684.

22. Kramer, S.L. (2006) *Geotechnical Earthquake Engineering*. Pearson Publishers.

23. Kristekova, M., Kristek, J., and Moczo, P. (2009) Time-frequency misfit and goodness-of-fit criteria for quantitative comparison of time signals. *Geophysical Journal International*, **178**, 813-825.